Journal of Telecommunication, Electronic and Computer Engineering
ISSN: 2180 – 1843 e-ISSN: 2289-8131 Vol. 18 No. 2 (2026) 1-8
jtec.utem.edu.my
DOI: https://doi.org/10.54554/jtec.2026.18.06.001

Assessment of Exposure from Wireless Devices: Multilayered Structure Method

Akram Gasmelseed
Department of Health Informatics, College of Applied Medical Sciences, Qassim University, 52571 Buraydah, Qassim, Saudi Arabia.

Article Info

Article history:
Received Mar 17th, 2025
Revised Apr 21st, 2026
Accepted Jun 3rd, 2026
Published Jun 30th, 2026

Index Terms:
Electromagnetic dosimetry
5G radiation safety
Fat tissue shielding
Multilayered tissue modeling

Abstract

Considering the recent breakthrough in wireless mobile telecommunications technology, there is need for more scientific and public awareness on the electromagnetic radiation risks associated with this growing technology. As, the human body is composed of biological tissues of complicated structures. This led to different behavior of biological tissue with respect to dosimetry-related research. The purpose of this study is to initially investigate the shielding properties of fat tissue against electromagnetic radiation. Furthermore, the study explores the biological effects of fifth generation (5G) communication devices operating in the 24.25 – 5.26 GHz frequency band on human head. Through simulation analysis, it founds that, for frequencies in the range 1–2 GHz, the fat tissue has the highest reflection coefficient values. However, this is not true for s-polarization with angle of incidence greater than 50°. Moreover, it is found in case of 5G irradiation that the highest power reflection coefficient (76.4%) is achieved for s-polarization with angle of incidence of 60° and appears at the lower frequency end of band FR2. On the other hand, the highest power transmission coefficient (85%) is achieved for p-polarization with angle of incidence of 60° and appears at the upper frequency end. Further, the values of the maximum temperature rise achieved for p-polarization of 30° and 60°, respectively. However, for frequencies greater than 36.4 GHz, the maximum temperature rise for normal incidence exceeds that of p-polarization with angle of incidence of 60°. Overall, the findings indicate that the amount of fat tissue should be carefully considered during the design of dosimetry experiments; under the simulated FR2 exposure conditions, 5G radiation did not produce adverse health effects in the modeled human-head tissue..

*Corresponding Author: a.mukhtar@qu.edu.sa

I. INTRODUCTION

With the recent breakthrough in wireless mobile telecommunications technology, there is need for more scientific and public awareness on the electromagnetic radiation risks associated with this growing technology [1].

This fact triggered many efforts made by several international bodies (e.g., IEEE, ICNIRP and WHO) which has been devoted to the elaboration of general guidelines limiting the electromagnetic radiation exposure from this technology (e.g., cell phone, Wi-Fi, etc.) [2]-[4]. These guidelines or limits were obtained through either laboratory studies [5, 6] or simulation results [7], [8]. Nowadays, due to ethical and legal constraints of using human or animal laboratory experiments, computer simulation play a critical role in implementing these guidelines [9].

The human body is composed of biological tissues of complicated structures. This led to different behavior of biological tissue with respect to dosimetry-related research. Prior research points out that there exists an electromagnetic shielding behavior of fat tissue at frequencies of 0.631, 0.9, 0.915 and 1.8 GHz, and states that the peak SAR, average SAR, and total power absorbed by the body with a fat layer are much lower than those without a fat layer [10]-[13].

On the other hand, for 5G radiation emitting devices, the electromagnetic energy absorption tends to be more superficial and concentrated [14]-[16]. Energy deposition could occur quickly in a smaller tissue area or mass, causing intense temperature elevation within a very short exposure period. Moreover, recent research shows no evidence for health risks associated with the exposure to 5G radiation and suggested to control the setup and operation of future experimental studies and to monitor the long-term epidemiological studies to identify health effects associated with exposure to wireless radiation [17]. Whereas other research suggested the use of lower frequencies for 5G up to 3.5 GHz because of no proven adverse health effects [18].

The purpose of this study is to initially investigate the shielding properties of fat tissue against electromagnetic radiation, and to further explore the biological effects of 5G communication devices on human head tissue. This paper employs a one-dimensional (1D) computer simulation to investigate these effects. The simulation model is developed

based on multilayered structure method. Although, several two- and three-dimensional methods exist to assess the risk of exposure to electromagnetic fields radiating from wireless telecommunications devices [19], [20], insights obtained from simple model simulations can draw important conclusions about the interaction of electromagnetic radiation with biological tissue as compared to more realistic and complicated models [21]. Further, 5G electromagnetic radiation is divided into two frequency bands which are Frequency Range 1 or FR1 (450-6000 MHz) and Frequency Range 2 or FR2 (24.25-5.26 GHz) [22]. This work focuses primarily on the induced biological effects of FR2 frequency band on human head. The paper shows how to use one-dimensional (1-D) multilayered structure to simulate biological model, as well as on how to calculate and measure the radiation exposure using MATLAB software.

II. METHODOLOGY

A. Interaction of Electromagnetic Waves with Biological tissues

The aim of this subsection is to introduce the basic governing equations used to describe and simulate numerically the propagation of electromagnetic waves in biological tissues. In the case of a linear homogeneous isotropic source-free and lossy dielectric medium, the time-harmonic Maxwell's equations describe the propagation of electromagnetic waves can be written as [23]:

$$\nabla \times \bar{E} = -j\omega\mu\bar{H} \tag{1}$$

$$\nabla \times \bar{H} = (\sigma + j\omega\varepsilon)\bar{E} \tag{2}$$

$$\nabla \cdot \bar{E} = 0 \tag{3}$$

$$\nabla \cdot \bar{H} = 0 \tag{4}$$

where $\bar{E}$ is the intensity of electric field (in V/m), $\bar{H}$ is the intensity of magnetic field (in A/m), j is imaginary constant ($\sqrt{-1}$), ω is the wave angular frequency of (in rad/s), σ is the conductivity of the medium (in S/m), ε is the permittivity of the medium (in F/m) and μ is the magnetic permeability of the medium (in H/m).

By combining Equations (1), (2) and (3), we obtain the wave equation for which is given as:

$$\nabla^2\bar{E} + k^2\bar{E} = 0 \tag{5}$$

where $k = \sqrt{\omega^2\mu\varepsilon - j\omega\mu\sigma}$, is the wave number. Then, if we assume that the wave travels in z-direction with the electric field oriented in the x-direction, we can write Equation (5) as:

$$\frac{d^2E_x}{dz^2} + k^2E_x = 0 \tag{6}$$

The general solution of this ordinary differential equation can be presented as:

$$E_x(z) = E_o^+e^{-jkz} + E_o^-e^{jkz} \tag{7}$$

Here, the field $E_x(z)$ is represented as a summation of two waves: a forward wave traveling in the positive z-direction $E_o^+e^{-jkz}$ and a backward wave propagating in the negative z-direction $E_o^-e^{jkz}$.

B. Dielectric Properties of Biological tissues

The mechanism of electromagnetic interaction with biological bodies influenced by the individual dielectric constants of biological tissues. These properties can be described by the so-called complex permittivity (ε^*) of biological tissues [24]. By rearranging Equation (2), we have:

$$\begin{aligned}\nabla \times \bar{H} &= (\sigma + j\omega\mu)\bar{E} \\ &= j\omega\left(\varepsilon + \frac{\sigma}{j\omega}\right)\bar{E} \\ &= j\omega\varepsilon^*\bar{E}\end{aligned} \tag{8}$$

with

$$\varepsilon^* = \varepsilon_o\varepsilon_r^* = \varepsilon_o(\varepsilon_r' - \varepsilon_r'') \tag{9}$$

where

$$\varepsilon_r^* = \varepsilon_r - j\frac{\sigma}{\omega\varepsilon_o} \tag{10}$$

Here, ε_r^* is the relative complex permittivity, $\varepsilon_r^{'}$ is real part of complex permittivity and is a measure of how much energy from an external electric field is stored in the biological tissues, ε_r is the dielectric constant or relative permittivity of tissues, and ε_o is the air permittivity (8.854×10^{-12} F/m). The imaginary part of permittivity $\varepsilon_r^{''}$ is the dielectric loss factor, which is a measure of the dissipation or loss of the biological tissues due to an external electric field, and are related to the conductivity σ by:

$$\varepsilon_r^* = \frac{\sigma}{\omega} \tag{11}$$

where, σ is the conductivity of the tissues (S/m), $\omega = 2\pi f$ is the angular frequency of the electromagnetic radiation (rad/s), and f is the frequency of the radiation [Hz].

Different dielectric models exist in literature for describing the dependency between the relative complex permittivity and the electromagnetic radiation frequency. In this paper, the 4-Cole-Cole model is employed to describe the behavior of the complex relative permittivity for biological tissues with respect to the frequency [25]. For this model, the complex relative permittivity is given by:

$$\varepsilon_r^*(\omega) = \varepsilon_\infty + \sum_{n=1}^{4}\frac{\Delta\varepsilon_n}{1 + [j\omega\tau]^{1-\alpha_n}} + \frac{\sigma}{j\omega\varepsilon_o} \tag{12}$$

Table 1
Cole-Cole Parameters [25], Density [26] and Heat Capacity [26] of Head Tissue

Parameters	Skin	Fat	Bone	Dura	CSF	Grey Matter	White Matter
ε_∞	4	2.5	2.5	4	4	4	4
$\Delta\varepsilon_1$	32	3	10	40	65	45	32
τ_1(ps)	7.234	7.958	13.263	7.958	7.958	7.958	7.958
α_1	0	0.2	0.2	0.15	0.1	0.1	0.1
$\Delta\varepsilon_2$	1100	15	180	200	40	400	100
τ_2 (ns)	32.481	15.915	79.577	7.958	1.592	15.915	7.958
α_2	0.2	0.1	0.2	0.1	0	0.15	0.1
σ_s	2.0E-4	0.01	0.02	0.5	2	0.02	0.02
$\Delta\varepsilon_3$	0.0	3.3E+4	5000	1.0E+4	0	2.0E+5	4.0E+4
τ_3 (μs)	159.155	159.155	159.155	159.155	159.155	106.103	53.052
α_3	0.2	0.05	0.2	0.2	0	0.22	0.3
$\Delta\varepsilon_4$	0	1.0E+7	1.0E+5	1.0E+6	0	45.0E+6	35.0E+6
τ_4 (ms)	15.915	7.958	15.915	15.915	15.915	5.305	7.958
α_4	0.2	0.01	0	0	0	0	0.02
ρ_i (kg/m^3)	1109	911	1908	1174	1007	1044.5	1041
C_i (J/(kg/°C))	3390.5	2348.33	1312.833	3364	4095.5	3695.8	3582.8

where ε_∞ is the relative permittivity at $\omega\tau \gg 1$, $\Delta\varepsilon_n = \varepsilon_s - \varepsilon_\infty$ is the magnitude of dispersion region, ε_s is the relative permittivity at $\omega\tau \ll 1$, τ is the relaxation time constant, α is a measure of the broadening of the dispersion and σ_s is the static ionic conductivity,
Table 1, lists the values of these parameters for a given tissue type discussed in this paper.

C. *Multilaytered Structure Method*

By considering the analogy between the multilayered structure and a uniform transmission line, the biological model can be represented by the planar geometry shown in Figure 1.

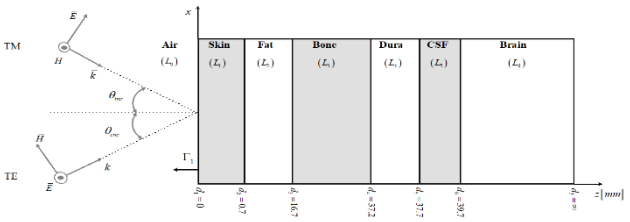

Figure 1. Multilayered structure of human head model

Hence, assuming the electromagnetic wave is a plane wave propagating in the positive *z*-direction at an angle ($\theta_i = \theta_{inc}$) relative to the negative *z*-axis, and with the electric field polarized linearly along the *x*-axis, then we can distinguish between two types of polarization of the incidence–wave: transverse electric (TE, or *s*-polarization) and transverse magnetic (TM, or *p*-polarization) polarization. In case of TE polarization, the electric field vector *E* is normal to the plane of incidence (*x*–*z* plane) and in case of TM polarization, the magnetic field vector *H* is normal to the plane of incidence. Thus, the radiated wave has a form similar to that of Equation (7), with the symbols E_o^+ and E_o^- being replaced by a_i and b_i, respectively. To simplify the analysis, the following variables are introduced: $\varphi_1 = x \cdot \sin\theta_i + z \cdot \cos\theta_i$ and $\varphi_2 = x \cdot \sin\theta_i - z \cdot \cos\theta_i$ which represent the phase terms for forward and backward propagation, respectively; and $\hat{u}_1 = \hat{x} \cdot \sin\theta_i - \hat{z} \cdot \cos\theta_i$ and $\hat{u}_2 = \hat{x} \cdot \sin\theta_i + \hat{z} \cdot \cos\theta_i$ which represent the directional vectors for forward and backward propagation, respectively. Hence, for TE polarization, the electric (E_i) and magnetic (H_i) fields in the i-th layer expressed as:

$$\bar{E}_i = (a_i e^{-jk_i\varphi_1} + b_i e^{-jk_i\varphi_2})\hat{y} \tag{13}$$

$$\bar{H}_i = -\hat{u}_1 \cdot \frac{a_i}{\eta_{TE_i}} e^{-jk_i\varphi_1} + \hat{u}_2 \cdot \frac{b_i}{\eta_{TE_i}} e^{-jk_i\varphi_2} \tag{14}$$

Similarly, for TM polarization, the electric and magnetic fields can be described as:

$$\bar{E}_i = \hat{u}_1 \cdot a_i e^{-jk_i\varphi_1} + \hat{u}_2 \cdot b_i e^{-jk_i\varphi_2} \tag{15}$$

$$\bar{E}_i = (a_i e^{-jk_i\varphi_1} + b_i e^{-jk_i\varphi_2}) / \eta_{TM_i} \cdot \hat{y} \tag{16}$$

Now, rewrite Equations (13)-(16) in general form, the transverse part may be expressed as:

$$\bar{E}_i = a_i e^{-jk_i z} + b_i e^{jk_i z} \tag{17}$$

$$\bar{H}_i = \frac{a_i e^{-jk_i z} - b_i e^{jk_i z}}{\eta_i} \tag{18}$$

where

$$k_i^2 = \omega^2 \mu_i \varepsilon_i - j\omega\mu_i\sigma_i \tag{19a}$$

$$\eta_i = \sqrt{\frac{\mu_i}{\varepsilon_i - j\frac{\sigma_i}{\omega}}} \tag{19b}$$

and

$$k_i^2 = k_{zi}^2 + k_x^2 \tag{20}$$

with

$$k_{zi} = k_i \cdot \cos\theta_i\,, \quad k_x = k_i \cdot \sin\theta_i \tag{21}$$

$$\eta_i = \eta_i / \cos\theta_i = \omega\mu_i / k_{zi} \quad \text{(TE case)} \quad (22)$$

$$\eta_i = \eta_i \cdot \cos\theta_i = k_{zi} / \omega\varepsilon_i \quad \text{(TM case)} \quad (23)$$

where

$$\cos\theta_i = \sqrt{1 - [\sin\theta_i]^2} = \sqrt{1 - \frac{k_1[\sin\theta_i]^2}{k_i}} \quad (24)$$

Further, one can then follow the derivation in [27] and obtain expression for the global reflection coefficient (Γ_i) at the layer interface $z = d_i$ given as:

$$\Gamma_i = \frac{Z_i - \eta_{i-1}}{Z_i + \eta_{i-1}} e^{-2jk_{i-1}d_i} \quad (25)$$

where the wave impedance (Z_i) is represented by:

$$Z_i = \eta_i \frac{1 + \Gamma_i e^{2jk_i d_i}}{1 - \Gamma_{i+1} e^{2jk_i d_i}} \quad (26)$$

After the induced electric field within the multilayered model is calculated, we can calculate the amount of power absorbed by the biological structure. The specific absorption rate (SAR) is defined as the amount of power absorbed per unit mass of the multilayered biological structure. The SAR is the primary dosimetric measures for determining exposure risk in the radiofrequency and microwave bands. Given the tissue density ρ_i (kg/m^3), the weighted averaged SAR for the tissue (W/kg) at the i-th layer is calculated as:

$$SAR_i = \frac{\sigma_i |E_i|^2}{2\rho_i} \quad (27)$$

where $|E_i|$ is the absolute value of the induced electric field (V/m) in the ith-layer. Additionally, Pennes bioheat equation is applied to describe the temperature rise due the irradiation of electromagnetic radiation. By neglecting the thermoregulatory response [28], the bioheat equation is expressed as:

$$T(t) = T_b + \frac{SAR_i}{\rho_b C_b \omega_b}\left[1 - e^{\frac{-\rho_b C_b \omega_b}{C_{tissue}}}\right] \quad (28)$$

where t is the time [mins], T_b is the ambient temperature of the body (= 36.6 ºC), ρ_b is the blood mass density (= 1050 kg/m^3), C_b is the blood heat capacity (= 3617 J/(kg/ºC)), ω_b is the blood perfusion rate (= 8.333*10^{-6} ml/g/min), C_{tissue} is the skin heat capacity (= 3391 J/(kg/ºC)).

III. IMPLEMENTATION

1) *Biological Model Structure*

The human head is modeled as comprising six tissue layers: skin, fat, bones, dura, cerebrospinal fluid (CSF) and brain. Figure 1 shows the structure of the model layers along with the associated thicknesses of each of the layers. The head model is assumed to be exposed to wireless electromagnetic fields at different frequencies power density of 5 W/m^2. The associated dielectric properties are given in Table 1 [25, 26].

2) *Dosimetry Parameters Programming*

We use Equation (19) to calculate the wave number k_i and characteristic impedance η_i, respectively. This calculation (shown in Figure 2) is done through for loop which will iterate from one till layers length. For the calculation of the reflection coefficients Equations (25) and (26), we used a decremented for loop that executes the calculations starting from the last layer using the impedance matching concept, as shown in Figure 3.

```
% updating coefficients
L = length(eps); % number of layers
for i=1:L
    epp(i) = sig(i)/omega;
    ep(i) = eps(i)*epsz;
    mu(i) = muz*mur(i);
    epsc(i) = ep(i) - 1i*epp(i); % complex
permittivity
    k(i) = omega*sqrt(muz*epsc(i)); % wave number
    eta(i) = sqrt(muz/epsc(i)); % characteristic
impedance
    n(i) = sqrt(epsc(i)/epsz); % index of
refraction
end
```

Figure 2. Calculations of wave number and characteristic impedance of the model, where the index of refraction is defined as $n = \sqrt{\varepsilon_r^* / \varepsilon_o}$

```
% reflection coefficients
G(L-1) = (eta(L)-eta(L-1))/(eta(L)+eta(L-1));
for i=L-1:-1:2
    Gama(i) = G(i)*exp(-1i*2*k(i)*d(i));
    z(i) = eta(i)*(1+Gama(i))/(1-Gama(i));
    G(i-1) = (z(i)-eta(i-1))/(z(i)+eta(i-1));
end
```

Figure 3. Calculations of the reflection coefficients

```
angle = 30; % incidence angle - degree
thr = angle*pi/180; % incidence angle - radiant

for i=1:L
    % determine cos(theta) by k:
    % cosinus(i) = sqrt(1-(k(1)/k(i)*sin(thr))^2);
    % or determine cos(theta) by n:
    cosinus(i) = sqrt(1-((sin(thr))^2/n(i)^2));
end

theta(1) = thr;
for i=2:L
    % determine theta(i)
    theta(i) = asin(n(i-1)/n(i)*sin(theta(i-1)));
end

kx = k(1)*sin(theta(1));
for i=1:L
    kz(i) = sqrt(k(i)^2 - kx^2); % =
k(i)*cosinus(i)

    % characteristic impedance:
    ntm(i) = n(i)*cosinus(i); % in case of TM
    nte(i) = n(i)/cosinus(i); % in case of TE
end
```

Figure 4. Calculations of wave number and characteristics impedance in case of oblique incident waves

Then, to program Equation (13) on a computer, one needs to use Equations (20)-(24) shown in Figure 4. Further, for a

power of 5 W/m^2, the associated incident electric field (a_1) is ~ 61.4 [V/m]. Thus, at each interface (d_i), we calculate the amplitudes of the incident wave (a_i), the reflected wave (b_i), and the electric field as shown in Figure 5.

```
i = 2;
r = -1*d(i);
a2 = (a1+b1)/(exp(-1i*k(i)*r)*(1+Gama(i)));
b2 = a2*G(2);

rr = 0.0;
Ex2 = a2*exp(-1i*k(i)*rr) + b2*exp(1i*k(i)*rr);
Ez2 = abs(Ex2);
```

Figure 5. Calculations of the incident and reflected amplitudes in the second layer

Further, the electric field distribution within each layer is calculated using a function called *fieldlines*. Then, we can determine the SAR distribution, as shown in Figure 6. The values for the tissue density used in this work are shown in Table 1, and the code snippet of *fieldlines* function is listed in Figure 7.

```
% SAR Distribution Computation
[Ezz2] = fieldlines(a2, b2, k(i), d(i)*10000,
d(i));
sar2 = 0.5*(sig(i)/(rho(i))).*(Ezz2.^2);
```

Figure 6. The function *fieldlines* utilized for computing the electric field and SAR

```
function [ez] = fieldlines(ai, bi, ki, delta,
strt)
    zz = 0.0;
    for i = 1:delta
        rr = -strt + zz;
        ex(i) = ai*exp(-1i*ki*rr) +
bi*exp(1i*ki*rr);
        et(i) = abs(ex(i));
        zz = zz + 0.0001;
    end
    ez = et;
end
```

Figure 7. The function *fieldlines* to compute the distribution of the electric field inside the multilayer structure

IV. RESULTS AND DISCUSSION

Figures. 8, 9 and 10 show the power reflection coefficients for TE and TM polarizations in the frequency range of 1 MHz–100 GHz with step 1 MHz, when the angle of incidence (θ_i) equals to 0^o, 30^o and 60^o, respectively.

As can be seen from Figures 8, 9 and 10(a), for frequencies in the range 1–2 GHz, the fat tissue has the highest reflection coefficient values. However, this is not true for perpendicular polarization with angle of incidence equal to 60^o, as shown in Figure 10(b). Thus, in order to further understand this behavior of perpendicular polarization reflection coefficients, another numerical experiment focusing on the frequency range between 10 MHz and 2.5 GHz and variable angle of incidence is investigated. Figure 11 shows the magnitude of power reflection coefficients.

For an incidence angles of 0° and 25° the magnitude of the reflectance of skin tissue is lower than the magnitude of the reflectance of fat tissue. As the incidence angle approach to 50^o, however, the s-polarized reflectance values were almost the same (27%) among skin and fat tissues. Thus, for incidence angles greater than 50^o, the reflectance of skin tissue becomes larger compared to that of the fat tissue (see Figure 11).

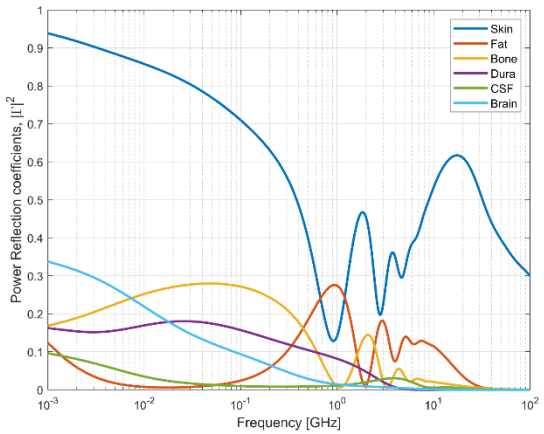

Figure 8. The Normal incidence ($\theta_i = 0^o$) power reflection coefficients, $|\Gamma^2|$

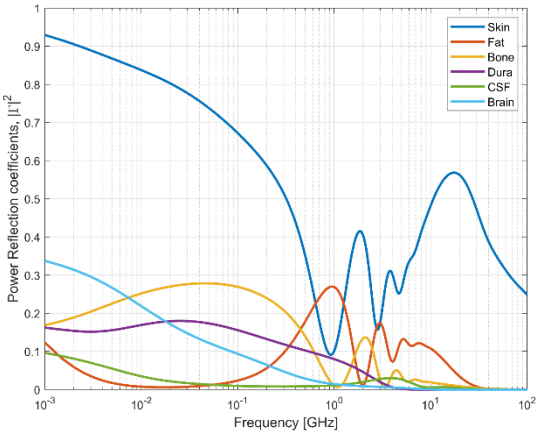

(a)

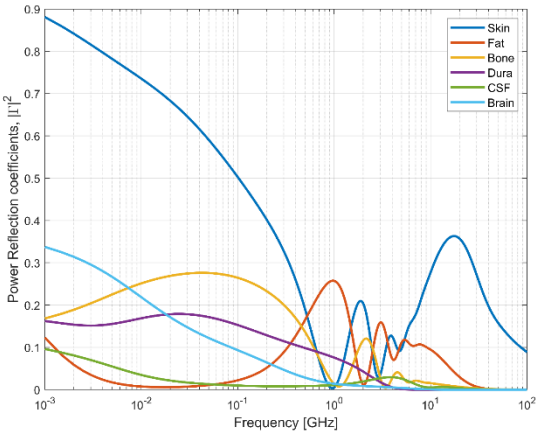

(b)

Figure 9. Power Reflection coefficients for TM polarization for incident angles: (a) $\theta_i = 30^o$ and (b) $\theta_i = 60^o$

To assess effects of 5G radiation, measurements were carried out in frequency range 24.25–52.6 GHz with step 0.5 MHz, Figure 12 shows the percentage of the power reflection ($|\Gamma^2|$) and transmission coefficients ($1 - |\Gamma^2|$) at the skin surface. It is found that the s-polarization has a higher power reflection coefficient as compared to p-polarization for frequency range of interest. Moreover, the highest power reflection coefficient (76.4%) is achieved for s-polarization (θ_i = 60^o) and appears at the lower frequency end of band

FR2. On the other hand, the highest power transmission coefficient (85%) is achieved for p-polarization polarization (θ_i = 60º) and appears at the upper frequency end.

Due to the highly superficial nature of 5G radiation energy for frequencies ranging from 24.25 GHz to 52.6 GHz (the penetration depth of the skin is ~0.1-0.5mm), most of radiation power is absorbed in the superficial layers of the human head.

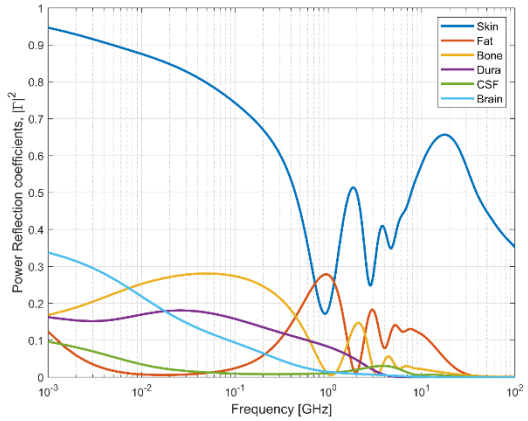

(a)

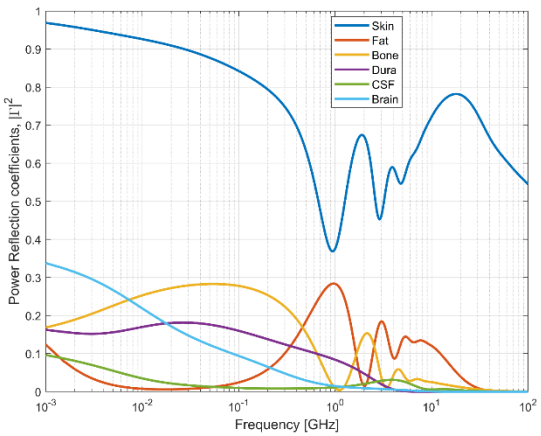

(b)

Figure 10. Power Reflection coefficients for TE polarization for incident angles: (a) θ_i = 30º and (b) θ_i = 60º

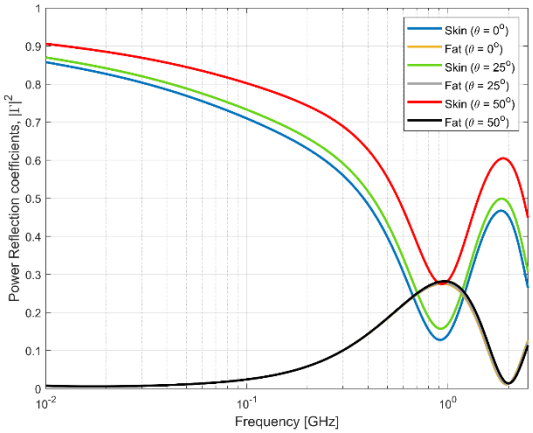

Figure 11. Power Reflection coefficients for TE polarization with variable angle of incidence

Figure 13 shows the predicted temperature rise in the skin tissue for the different polarizations. The maximum percentage increase in the temperature, for the different polarizations, is 0.6%.

The values of the maximum temperature rise achieved for p-polarization of 30º and 60º, respectively. However, for frequencies greater than 36.4 GHz, the temperature rise for

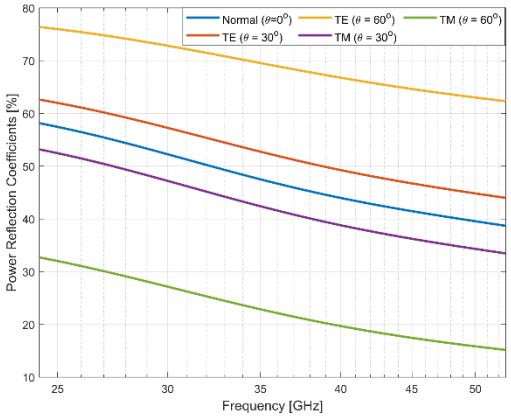

(a)

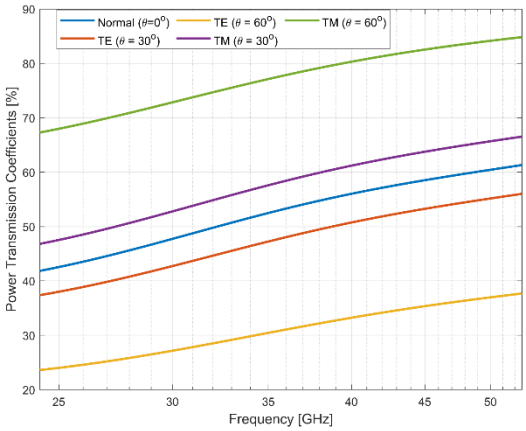

(b)

Figure 12. Percentage of (a) Power Reflection and (b) power transmission coefficients

normal incidence exceeds that of p-polarization of 60º. Moreover, the maximum temperature rise in the internal tissue of the human head regions is found to be rather negligible. Fig. 14 shows the predicted temperature rise in the brain tissue for the different polarizations.

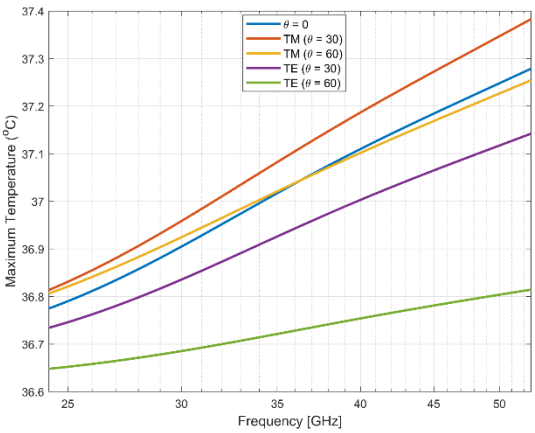

Figure 13. Maximum temperature versus frequency for the skin tissue

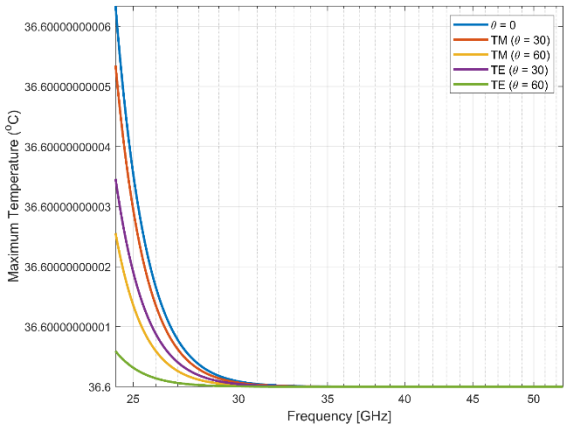

Figure 14. Maximum temperature versus frequency for the brain tissue

V. CONCLUSION

This paper initially investigates the shielding properties of fat tissue against electromagnetic radiation. Then, the paper explores the biological effects of fifth generation (5G) communication devices operating in the 24.25 – 52.6 GHz frequency band on human head.

Through simulation analysis, it founds that, for frequencies in the range 1–2 GHz, the fat tissue has the highest reflection coefficient values. However, this is not true for s-polarization with angle of incidence greater than 50º.

Moreover, it is found in case of 5G irradiation that the highest power reflection coefficient (76.4%) is achieved for s-polarization (θ_i = 60º) and appears at the lower frequency end of band FR2. On the other hand, the highest power transmission coefficient (85%) is achieved for p-polarization (θ_i = 60º) and appears at the upper frequency end. Further, the values of the maximum temperature rise achieved for p-polarization of 30º and 60º, respectively. However, for frequencies greater than 36.4 GHz, the temperature rise for normal incidence exceeds that of p-polarization of 60º.

Accordingly, the amount of fat tissue should be carefully considered during the design of dosimetry experiments. Under the simulated exposure conditions, 5G radiation in the FR2 band did not produce adverse health effects in the modeled human-head tissue..

CONFLICT OF INTEREST

Author declares that there is no conflict of interests regarding the publication of the paper.

AUTHOR CONTRIBUTION

The author solely responsible for all aspects of the study: conception and design, data collection, analysis and interpretation of findings, and manuscript preparation.

REFERENCES

[1] A C. L. Russell, "5G wireless telecommunications expansion: Public health and environmental implications," Environ. Res., vol. 165, pp. 484-495, 2018, https://doi.org/10.1016/j.envres.2018.01.016

[2] International Commission on Non-Ionizing Radiation Protection (ICNIRP), "Guidelines for limiting exposure to electromagnetic fields (100 kHz to 300 GHz)," Health Phys., vol. 118, no. 5, pp. 483-524, 2020, https://doi.org/10.1097/HP.0000000000001210

[3] "IEEE Standard for Safety Levels with Respect to Human Exposure to Electric, Magnetic, and Electromagnetic Fields, 0 Hz to 300 GHz," IEEE Std C95.1-2019 (Revision of IEEE Std C95.1-2005/ Incorporates IEEE Std C95.1-2019/Cor 1-2019), pp. 1-312, 2019, https://doi.org/10.1109/IEEESTD.2019.8859679

[4] R. F. Cleveland, "Guidelines for Radiofrequency Exposure from Mobile and Portable Devices Adopted by the US Federal Communications Commission," in Wireless Phones And Health II, G. L. Carlo and P. M. Thibodeau, Eds., Boston, MA, USA: Springer, 2002, pp. 101-106, https://doi.org/10.1007/0-306-46901-4_6

[5] M. Capstick, Y. Gong, B. Pasche and N.Kuster, "An HF exposure system for mice with improved efficiency," Bioelectromagnetics, vol. 37, no. 4, pp. 223-233, 2016, https://doi.org/10.1002/bem.21969

[6] Y. Gong, M. H. Capstick, S. Kuehn; P. F. Wilson, J. M. Ladbury and G. Koepke, "Life-Time Dosimetric Assessment for Mice and Rats Exposed in Reverberation Chambers for the Two-Year NTP Cancer Bioassay Study on Cell Phone Radiation," IEEE Trans. Electromagn. Compat., vol. 59, no. 6, pp. 1798-1808, 2017, https://doi.org/10.1109/TEMC.2017.2665039

[7] T. Nagaoka et al., "Development of realistic high-resolution whole-body voxel models of Japanese adult males and females of average height and weight, and application of models to radio-frequency electromagnetic-field dosimetry," Phys. Med. Biol., vol. 49, no. 1, pp. 1, 2003, https://doi.org/10.1088/0031-9155/49/1/001

[8] A. D. Tinniswood, C. M. Furse and O.P. Gandhi, "Power deposition in the head and neck of an anatomically based human body model for plane wave exposures," Phys. Med. Biol., vol. 43, no. 8, pp. 2361, 1998, https://doi.org/10.1088/0031-9155/43/8/026

[9] A. K. Kiani et al., "Ethical considerations regarding animal experimentation," J. Prev. Med. Hyg., vol. 63, no. 2 Suppl 3, pp. E255-E266, 2022, https://doi.org/10.15167/2421-4248/jpmh2022.63.2S3.2768

[10] H.-R. Chuang, "Numerical computation of fat layer effects on microwave near-field radiation to the abdomen of a full-scale human body model," IEEE Trans. Microw. Theory Tech., vol. 45, no. 1, pp. 118-125, 1997, https://doi.org/10.1109/22.552040

[11] L. . -C. Kuo, C. . -C. Lin and H. . -R. Chuang, "FDTD computation of fat layer effects on SAR distribution in a multilayered superquadric-ellipsoidal head model and MRI-based heads proximate to a dipole antenna," in APRASC, 2004, pp. 528-, https://doi.org/10.1109/APRASC.2004.1422545

[12] C. K. Chou, J. A. McDougall, K. W. Chan and K.H. Luk, "Effects of fat thickness on heating patterns of the microwave applicator MA-151 at 631 and 915 MHz," Int. J. Radiat. Oncol. Biol. Phys., vol. 19, no. 4, pp. 1067-1070, 1990, https://doi.org/10.1016/0360-3016(90)90035-I

[13] Liang-Chen Kuo and Huey-Ru Chuang, "FDTD computation of fat layer effects on the SAR distribution in a multilayered superquadric-ellipsoidal head - model irradiated by a dipole antenna at 900/1800 MHz," in IEEE/EMC '03, 2003, pp. 323-326 Vol.1, https://doi.org/10.1109/ICSMC2.2003.1428256

[14] J. C. Lin, "FCC Announces Its Existing RF Exposure Limits Apply to 5G [Health Matters]," in IEEE Microwave Magazine, vol. 21, no. 4, pp. 15-17, April 2020, https://doi.org/10.1109/MMM.2019.2963754

[15] K. R. Foster, M. C. Ziskin and Q. Balzano, "Time-temperature Thresholds and Safety Factors for Thermal Hazards from Radiofrequency Energy above 6 GHz," Health Phys., vol. 121, no. 3, pp. 234-247, 2021, https://doi.org/10.1097/HP.0000000000001447

[16] M. S. Morelli, S. Gallucci, B. Siervo and V, Hartwig, "Numerical Analysis of Electromagnetic Field Exposure from 5G Mobile Communications at 28 GHZ in Adults and Children Users for Real-World Exposure Scenarios," Int. J. Environ. Res. Public Health, vol. 18, no. 3, pp. 1073, 2021, https://doi.org/10.3390/ijerph18031073

[17] L. Hardell, "Health Council of the Netherlands and evaluation of the fifth generation, 5G, for wireless communication and cancer risks," World J. Clin. Oncol., vol. 12, no. 6, pp. 393-403, 2021, https://doi.org/10.5306/wjco.v12.i6.393

[18] S. C. DeMarco, G. Lazzi, Wentai Liu, J. D. Weiland and M. S. Humayun, "Computed SAR and thermal elevation in a 0.25-mm 2-D model of the human eye and head in response to an implanted retinal stimulator - part I: models and methods," in IEEE Transactions on Antennas and Propagation, vol. 51, no. 9, pp. 2274-2285, Sept. 2003, https://doi.org/10.1109/TAP.2003.816395

[19] G. Lazzi, S. C. DeMarco, Wentai Liu, J. D. Weiland and M. S. Humayun,, "Computed SAR and thermal elevation in a 0.25-mm 2-D model of the human eye and head in response to an implanted retinal stimulator - part II: results," in IEEE Transactions on Antennas and Propagation, vol. 51, no. 9, pp. 2286-2295, Sept. 2003, https://doi.org/10.1109/TAP.2003.816394

[20] E. Aguilera, N. M. Peña and J. C. Bohórquez, "Heating within Spheres of Different Size Irradiated by an Electromagnetic Plane Wave," in IEEE Latin America Transactions, vol. 8, no. 6, pp. 618-622, Dec. 2010, https://doi.org/10.1109/TLA.2010.5688086

[21] T. Samaras, A. Christ, A. Klingenbock and N. Kuster, "Worst Case Temperature Rise in a One-Dimensional Tissue Model Exposed to Radiofrequency Radiation," in IEEE Transactions on Biomedical Engineering, vol. 54, no. 3, pp. 492-496, March 2007, https://doi.org/10.1109/TBME.2006.890498

[22] L. Yu et al., "Sparse Code Multiple Access for 6G Wireless Communication Networks: Recent Advances and Future Directions," in IEEE Communications Standards Magazine, vol. 5, no. 2, pp. 92-99, June 2021, https://doi.org/10.1109/MCOMSTD.001.2000049

[23] C. Hazard and M. Lenoir, "On the Solution of Time-Harmonic Scattering Problems for Maxwell's Equations," SIAM J. Math. Anal., vol. 27, no. 6, pp. 1597-1630, 1996, https://doi.org/10.1137/S0036141094271259

[24] L. Farrugia et al., "The Complex Permittivity of Biological Tissues: A Practical Measurement Guideline," in IEEE Access, vol. 12, pp. 10296-10314, 2024, https://doi.org/10.1109/ACCESS.2024.3352728

[25] S. Gabriel, R, W, Lau and C, Gabriel, "The dielectric properties of biological tissues: II. Measurements in the frequency range 10 Hz to 20 GHz," Phys. Med. Biol., vol. 41, no. 11, pp. 2251, 1996, https://doi.org/10.1088/0031-9155/41/11/002

[26] IT'IS Foundation, "Tissue Properties Database V4.0," Accessed: Feb. 21, 2025, [Online]. Available: https://itis.swiss/virtual-population/tissue-properties/, https://doi.org/10.13099/VIP21000-04-0

[27] A. Gasmelseed, "New Development Environment for Modern Bioelectromagnetics Signal Processing Applications [Application Notes]," in IEEE Microwave Magazine, vol. 14, no. 5, pp. 134-152, July-Aug. 2013, https://doi.org/10.1109/MMM.2013.2259404

[28] T. B. Rashid and H. H. Song, "Analysis of biological effects of cell phone radiation on human body using specific absorption rate and thermoregulatory response," Microw. Opt. Technol. Lett., vol. 61, no. 6, pp. 1482-1490, 2019, https://doi.org/10.1002/mop.31777.